Materials Today Bio 19 (2023) 100610

Contents lists available at ScienceDirect

Materials Today Bio

journal homepage: www.journals.elsevier.com/materials-today-bio

A mesoporous polydopamine-derived nanomedicine for targeted and synergistic treatment of inflammatory bowel disease by pH-Responsive drug release and ROS scavenging

Haidi Guan [a,1], Zhongwei Xu [a,1], Guangsheng Du [a,1], Qinghua Liu [a], Qianshan Tan [a], Yihui Chen [a], Shuaishuai Chen [a], Jingfeng Wu [b,c], Fengchao Wang [c], Jixi Zhang [d,***], Lihua Sun [a,*], Weidong Xiao [a,**]

[a] Department of General Surgery, Xinqiao Hospital, Army Medical University, No.183 Xinqiao Road, Chongqing, 400037, China
[b] Department of Gastroenterology, Southwest Hospital, Army Medical University, Gaotanyan Street, Shapingba, Chongqing, 400038, China
[c] Institute of Combined Injury of PLA, State Key Laboratory of Trauma, Burns and Combined Injury, Army Medical University, Gaotanyan Street, Shapingba, Chongqing, 400038, China
[d] Key Laboratory of Biorheological Science and Technology, Ministry of Education, College of Bioengineering, Chongqing University, No. 174 Shazheng Road, Chongqing, 400044, China

ARTICLE INFO

Keywords:
Inflammation bowel disease
Mesoporous polydopamine nanomedicine
pH-responsive drug release
ROS scavenging
Synergetic therapy

ABSTRACT

Repurposing clinically approved drugs to construct novel nanomedicines is currently a very attractive therapeutic approach. Selective enrichment of anti-inflammatory drugs and reactive oxygen species (ROS) scavenging at the region of inflammation by stimuli-responsive oral nanomedicine is an effective strategy for the treatment of inflammatory bowel disease (IBD). This study reports a novel nanomedicine, which is based on the excellent drug loading and free radical scavenging ability of mesoporous polydopamine nanoparticles (MPDA NPs). By initiating polyacrylic acid (PAA) polymerization on its surface, a "core-shell" structure nano-carrier with pH response is constructed. Then, under alkaline conditions, using the π-π stacking and hydrophobic interaction between the anti-inflammatory drug sulfasalazine (SAP) and MPDA, the nanomedicines (PAA@MPDA-SAP NPs) loaded efficiently (928 μ g mg^{-1}) of SAP was successfully formed. Our results reveal that PAA@MPDA-SAP NPs can pass through the upper digestive tract smoothly and finally accumulate in the inflamed colon. Through the synergistic effect of anti-inflammation and antioxidation, it can effectively reduce the expression of pro-inflammatory factors and enhance the intestinal mucosal barrier, and finally significantly alleviate the symptoms of colitis in mice. Furthermore, we confirmed that PAA@MPDA-SAP NPs have good biocompatibility and anti-inflammatory repair ability under inflammation induction through human colonic organoids. In summary, this work provides a theoretical basis for the development of nanomedicines for IBD therapy.

1. Introduction

Inflammatory bowel disease (IBD) is a chronic relapsing idiopathic autoimmune disease characterized by epithelial barrier dysfunction and intestinal ulceration, seriously affects the quality life of patients [1–3]. It is a global disease and the incidence is increasing internationally, particularly in nations with historically low rates [4,5]. Although sustained clinical remission has recently been recognized as an important goal of IBD therapy, there are not many treatment options to maintain long-term remission. Conventional treatment consists of mainly trying to control symptoms with high doses of drugs, such as amino-salicylates, corticosteroids, immunomodulators, and biologics. Sulfasalazine (SAP) is a small molecule oral drug with good anti-inflammatory effect commonly used for IBD. However, a significant number of patients do not respond to current treatments or do not benefit from it due to long-term systemic nonspecific distribution of SAP owing to multiple adverse

* Corresponding author.
** Corresponding author.
*** Corresponding author.
E-mail addresses: jixizhang@cqu.edu.cn (J. Zhang), slh6260@163.com (L. Sun), xiaoweidong@tmmu.edu.cn (W. Xiao).
[1] These authors contributed equally.

https://doi.org/10.1016/j.mtbio.2023.100610
Received 25 December 2022; Received in revised form 24 February 2023; Accepted 11 March 2023
Available online 15 March 2023
2590-0064/© 2023 The Authors. Published by Elsevier Ltd. This is an open access article under the CC BY-NC-ND license (http://creativecommons.org/licenses/by-nc-nd/4.0/).

effects [6–8]. Therefore, targeted drug delivery to the region of inflammation in the colon should be beneficial to avoiding the undesirable systemic toxicity caused by nonspecific distribution of drug and improving treatment efficiency [9–12]. Based on the epithelial enhanced permeation and retention effect (eEPR) in inflammatory tissues, recent studies focus on the strategies for delivering drugs to the inflammatory site explicitly by employing nanoparticles-based oral formulations [13–15].

In addition, reactive oxygen species (ROS) produced in mitochondria distinctly contribute to inflammation response and oxidative stress accelerates the development of IBD. In recent years, numerous efforts have explored the nanomedicine with ROS scavenging activity for the treatment of IBD [16–20]. However, based on the complex pathogenesis and molecular interactions of IBD among the different proinflammatory cytokines/chemokines, oxidative mediators, inflammatory cells, and immune cells, few mono-therapies deliver satisfactory effects against IBD in the long-term [9,21]. Fortunately, several categories of nanoscale medicines have been designed for co-administration of anti-inflammatory drugs and ROS scavenging for treatment of IBD, which can simultaneously scavenge excessive ROS and deliver anti-inflammatory drugs to inhibit the production of inflammatory cytokines may lead to improved therapeutic effects. For example, Qiu et al. reported a hollow MnO_2 nanozymes to deliver budesonide for synergistic treatment of IBD [22] and Lin et al. reported a Mn doped prussian blue nanozymes (MPBs) to directly deliver SAP for synergistic treatment of IBD [23]. It inspired us to develop a strategy that can effectively remove the reactive oxygen species and achieve higher drug accumulation in the inflamed colon region simultaneously, thus improving the therapeutic performance against IBD.

Polydopamine (PDA), a black insoluble biopolymer produced by autoxidation of the catecholamine neurotransmitter with good biocompatibility and widely used in biomedicine [24,25]. PDA with abundant reductive groups, such as phenol and catechol, is endowed with excellent redox ability in alleviating oxidative stress (free radical scavenging) by liberating electrons, which may act as a potential ROS scavenger [26,27]. Mesoporous polydopamine nanoparticles (MPDA NPs) in comparison to the nonporous counter-parts can provide high accessibility of the active sites and have attracted considerable attention [28–33].

Herein, we developed a synergistic therapy system (PAA@MPDA-SAP NPs) for IBD treatment by utilizing MPDA as the drug carrier and ROS scavenger and polyacrylic acid (PAA) as the "molecular switch". As shown in Fig. 1a. To realize the efficient delivery of SAP, MPDA NPs of a size about 90 nm were prepared, and then a protective shell of PAA was modified on the surface of the MPDA NPs via catalysis of APS. The PAA could function as a "gate" to prevent the degradation and early release of the drugs in the stomach after oral administration. In this way, the and morphological changes of PAA in the gastrointestinal environment is utilized to achieve the efficient enrichment of SAP in the region of inflammation. As shown in Fig. 1b, the synergistic effect of PAA@MPDA-SAP NPs were fully explored. The therapeutic effect of DSS-induced colitis was evaluated together with the exploration of the synergistic mechanism, while the biosafety was evaluated both in vitro and in vivo.

2. Experimental

2.1. Synthesis of PAA@MPDA NPs

PAA@MPDA NPs was synthesized as follows. In a typical synthesis, MPDA (8 mg) was dissolved into HEPES (25 mL, pH 7.2) containing of acrylic acid (AA, 3 mL). After stirring at room temperature for 30 min, the reaction temperature was raised to 50 °C, and ammonium persulphate (APS, 200 mg) dissolved in deionized water (1 mL) was injected into the reaction mixture under nitrogen. The reaction was carried out at 50 °C for 3 h. The weight ratio of the reactants was 1 MPDA/0.1375 Acrylic acid (AA)/25 APS. Finally, the reaction product (nanoparticles) was separated by centrifugation. Ethanol and acetone were used to wash the centrifuged particles. The template removal was performed by extraction, where the samples were treated in a mixed solution of ethanol and acetone (2:1 v/v) by sonication (three times, 30 min each time). The final product was obtained by dialysis against water for three days.

2.2. Colloidal stability study of PAA@MPDA NPs

To investigate the suspension stability of the PAA@MPDA NPs, PAA@MPDA NPs were dispersed with simulated gastric fluid (SGF, pH 1.2), simulated intestinal fluid (SIF, pH 7.0), DMEM media and FBS for 24 h and 48 h, then the hydrodynamic diameter distributions were measured by dynamic light scattering (DLS) techniques using a Zetasizer Nano instrument at room temperature. The long-term hydrodynamic stability (96 h) of PAA@MPDA NPs at water was also monitored by DLS

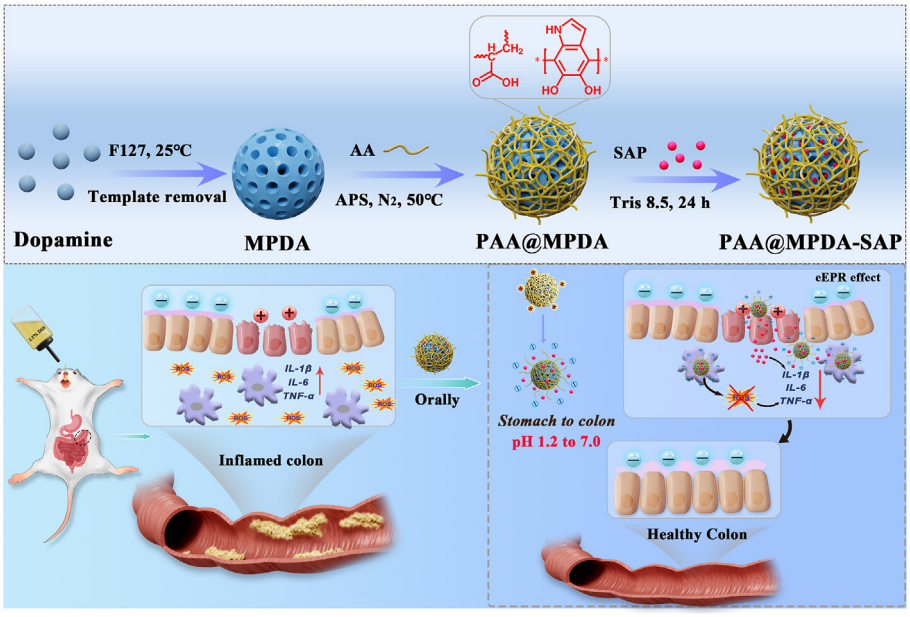

Fig. 1. Design of the PAA@MPDA-SAP NPs for inflammation bowel disease treatment. (a) Schematic for the fabrication of PAA@MPDA-SAP NPs (b) PAA@MPDA-SAP enriched in colonic inflammatory sites to scavenge excessive ROS and release loaded SAP for synergistic IBD therapy.

techniques. Furthermore, the TEM was used to observe the morphology stability of the PAA@MPDA NPs under SGF and SIF for 24 h.

2.3. Sulfasalazine (SAP) loading and release profile of PAA@MPDA NPs

For the determination of the adsorption isotherm of SAP, PAA@MPDA NPs (2 mg) were dispersed ultrasonically in the drug solution (2 mL) of tris buffer (25 mM, pH 8.5) at various concentrations. The mixture was stirred at room temperature for 24 h and then centrifuged (11,000 rpm, 15 min) to collect the drug-loaded nanoparticles. The amount of drug loaded into the PAA@MPDA NPs was calculated by subtracting the mass of drug in the supernatant from the total mass of drug in the initial solution. The concentrations of the drugs in the solutions were analyzed by UV–vis spectrophotometry (NanoDrop 2000, Thermo) at a wavelength of 359 nm (SAP) [34].

The drug release experiments were performed to simulate the transport process in vivo after oral administration. First, 2 mg of drug-loaded nanoparticles were dispersed in SGF (2 mL) buffer for 2 h. Then, the above reaction mixture was centrifuged and dispersed into 2-(4-Morpholino) ethanesulfonic acid (MES, pH 4.5) for 4 h (2–5 h). Finally, the reaction mixture was centrifuged and the collected particles were dispersed into SIF buffer for various times (5–120 h). At the predetermined time intervals, solution (0.2 mL) was withdrawn from the solution, and the amount of released drug was analyzed by UV–vis. To maintain a constant volume, fresh medium (0.2 mL) was added after each sampling. All drug release results were based on an average of three measurements. The drug loading and release amount of SAP were calculated in the same way as in a previous study [35].

2.4. Assay for radical scavenging by the PAA@MPDA NPs

To investigate the Radical Scavenging stability of the PAA@MPDA NPs, DPPH was dissolved in 95% ethanol (100 mM) to form the mother liquor. Then, PAA@MPDA NPs of varying concentrations (0–20 μg mL^{-1}) were co-incubated with DPPH for 20 min (in dark). Finally, the UV–vis absorbance at 516 nm was recorded. Three replicate samples were prepared for each group. Moreover, for the •OH assay, the •OH radical scavenging activity of PAA@MPDA NPs was monitored using ABTS. First, H_2O (920 μL), varying concentrations of PAA@MPDA NPs (0–100 μg mL^{-1}), H_2O_2 (200 μM, 10 μL), and $FeSO_4{\cdot}7H_2O$ (18 mM, 20 μL) were mixed together. After ultrasonic treatment for 5 min, the supernatant was collected by centrifugation and then incubated with ABTS (10 μM, 50 μL) for another 3–5 min. Finally, the UV–vis absorbance at 800 nm was recorded to evaluate the antioxidant activity.

2.5. Human colon organoids culture

Six specimens of organoids were obtained from colon tissue which were collected from the General Surgery of Xinqiao Hospital. The experiments were carried out in strict accordance with the regulations of the Institutional Human Ethics and User Committee of China and approved by the Medical Ethics Committee of Second Affiliated Hospital of Army Medical University (Ethics Number: 2022-YD104-01). First, colon cells were isolated from the collected colonic tissue according to a previous study. Then, the cells were centrifuged at 200 g for 5 min at 4 °C and the cell pellet was resuspended by a pre-chilled pipette tip with 50 μL of the Cultrex RGF BME (R&D Systems Cat. No. 3533-005-02)/gastric cell suspension mixture which was added to the center of each well of a 24-well plate. After placing the plate in an incubator at 37 °C for 25 min to allow the Cultrex RGF BME to solidify, an appropriate volume of gastric organoid expansion medium (approximately 500 μL per well of a 24-well plate) was added. Finally, the plate containing the organoid culture was returned to the cell incubator to promote organoid growth and the medium was subsequently refreshed every 2−3 day [36].

2.6. Animal studies

The anesthetic, surgical, and post-operative care protocols were examined and approved by the Animal Ethics Committee of Army Medical University (AMUWEC20224611). The colitis model of mice (C57BL/6, 8-week-old, male, 20–25 g) used was from the Experiment Animal Center of the Army Medical University.

2.7. Statistical analysis

The data were expressed as the mean ± SD for at least three independent replicates. The student t-test was performed for comparisons between two groups. The one-way ANOVA was performed for multiple groups. $P < 0.0001$ and $P < 0.05$ was considered statistically significant.

3. Results and discussion

3.1. Fabrication and characterization of PAA@MPDA NPs

MPDA NPs were fabricated according to the procedure reported in previous study with minor modifications [32]. The scanning electron microscopy (SEM) images and transmission electron microscope (TEM) images of MPDA revealed a size distribution of 90 ± 10 nm with a regularly ordered pore structure (Fig. 2a). Polyacrylic acid (PAA) has previously been used as a pH-responsive polymer for modifying and functionalizing different types of nanoparticles (NPs) for therapeutic intentions [37–40]. In this study, we constructed a pH-responsive "core-shell" nanocarrier (PAA@MPDA NPs) by using the interaction between PAA and PDA. PAA modified MPDA NPs (PAA@MPDANPs) had larger particle size (~110 nm), smaller pore size or direct plugging (Fig. 2b). The change in morphology was also confirmed by nitrogen adsorption and pore size distribution measurement. Compared with MPDA, the specific area and pore volume of PAA@MPDA decreased from 43.7 $m^2\ g^{-1}$ to 0.1 $cm^3\ g^{-1}$ to 14.7 $m^2\ g^{-1}$ and 0.03 $cm^3\ g^{-1}$, respectively (Fig. 2c). Moreover, HAADF STEM, X-ray photoelectron spectroscopy (XPS), infrared spectroscopy (FTIR), and thermogravimetric analysis (TGA) were used to further study the specific composition of the PAA@MPDA NPs. The coexistence of C, N, and O was confirmed by element mapping (Fig. S1) and XPS analysis (Fig. 2d). The C1s XPS spectra for PAA@MPDA NPs revealed a peak at 288.6 eV, which may be assigned to the O–C═O bonds in the PAA chain (Fig. 2e) [25].

The coating of PAA on the surface of MPDA was confirmed by FTIR spectroscopy (Fig. 2f). In the case without crosslinking, the strong adsorptions at 3249 cm^{-1} (stretching vibration of phenolic O–H) and 1563 cm^{-1} (stretching vibration of the aromatic ring and bending vibration of N–H) are the characteristic absorption peaks of MPDA, respectively. For the cross-linked case, the bands at 3102 cm^{-1} (stretching vibrations of asymmetric C–H) and 1724 cm^{-1} (stretching vibrations of C═O) are the basic characteristic absorption bands of PAA. In addition, the peak at 1619 cm^{-1} corresponds to the stretching vibration of C═O in the amide, confirming the occurrence of a cross-linking reaction between the carboxyl groups of the PAA binder and the amino groups of the PDA [41]. Moreover, the content of PAA (about 24%) in PAA@MPDA NPs was measured by TGA (Fig. 2g).

Studies showed that there are a large number of positively charged proteins in inflammatory colon. Negatively charged nanoparticles can be efficiently enriched in inflammatory colon tissue [42,43]. The zeta potential and the hydrodynamic diameter distributions of the PAA@MPDA NPs were examined. As shown in Fig. 2h and i, compared with MPDA NPs (−14.1 mV), the zeta potential of PAA@MPDA NPs was decreased to −50.7 mV. The hydrodynamic diameter distributions of PAA@MPDA NPs have increased to ~130 nm because of the presence of a hydrated layer around the particles. In addition, the long-term hydrodynamic stability was also decreased in Fig. S2. Meanwhile, The optimal weight ratio of PAA to MPDA in the nanocarriers was determined by zeta potential and hydrodynamic diameter distributions. The results showed

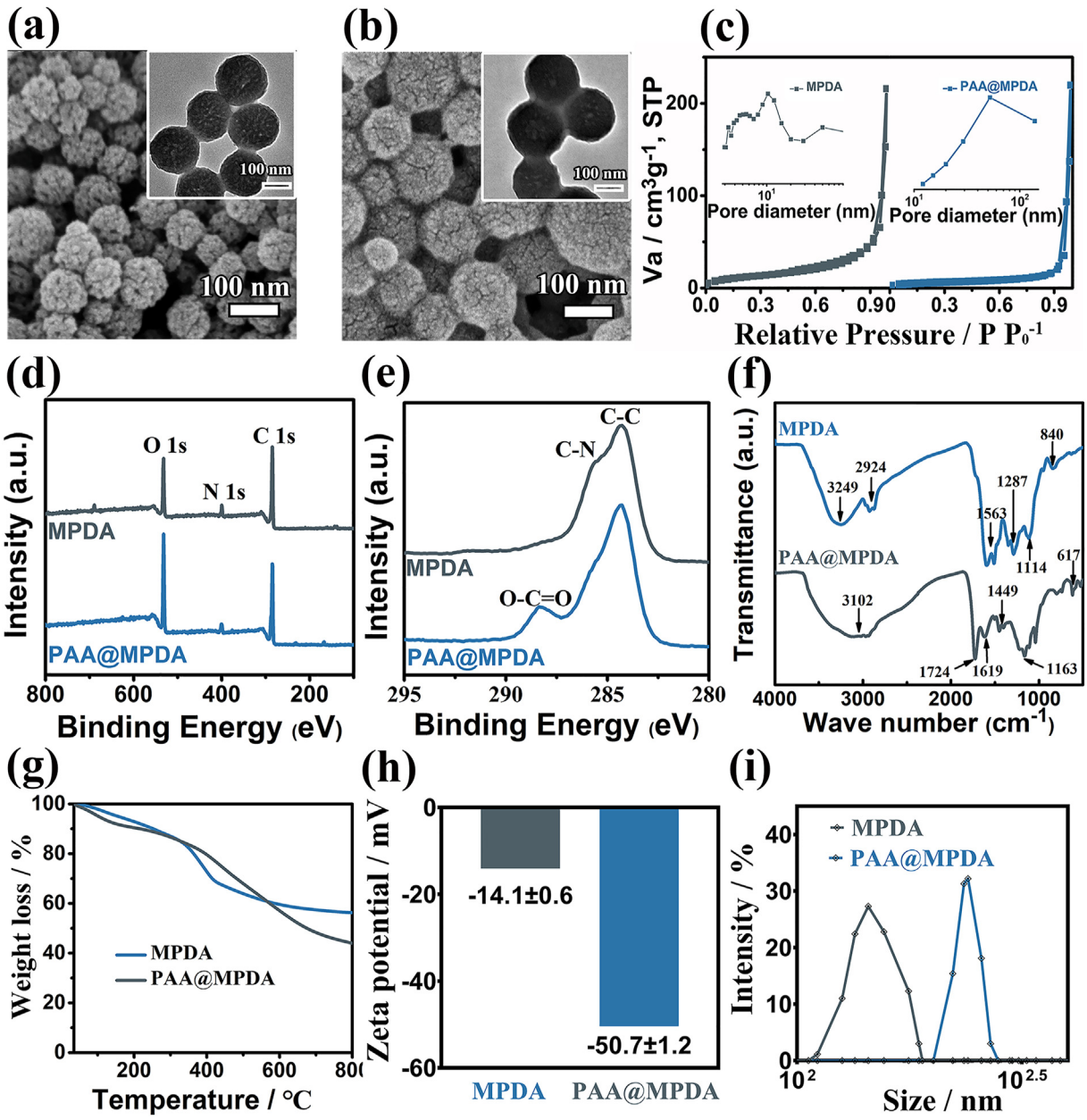

Fig. 2. Characterization of MPDA and PAA@MPDA NPs. SEM images of (a) MPDA NPs and (b) PAA@MPDA NPs. Inset: the close-up TEM image of MPDA NPs and PAA@MPDA NPs. (c) N_2 adsorption–desorption isotherms and corresponding pore size distributions. (d, e) XPS survey of the as-prepared NPs as well as the high-resolution scans of C 1s. (f) FTIR, (g) TGA curves, (h) Zeta potential, (i) Dynamic light scattering (DLS) data of MPDA NPs and PAA@MPDA NPs.

that the PAA formed a shell uniformly by synthesis at the optimized MPDA/Acrylic acid (AA) weight ratio of 2.4, while an increase (7.3, 3.6) or decrease (1.8) of the ratio led to less PAA compound and a larger size of nanoparticles (Fig. S3). These results suggest the successful preparation of the core-shell nanoparticles (PAA@MPDA NPs).

3.2. ROS scavenging, drug-loading, and releasing capacity of PAA@MPDA NPs

Polydopamine (PDA) is abundant with the abundant reductive pendant groups, such as phenol, catechol, and imine, which enable PDA to scavenge multiple ROS effectively for the treatment of inflammation-induced injuries both in vitro and in vivo [28]. PDA-based nanoparticles have also been used as an antioxidant in ROS scavenging in research on anti-inflammation. In this study, the ROS scavenging activity of PAA@MPDA NPs toward DPPH,•OH, and $\bullet O_2^-$, was investigated by using a ROS probe (DPPH/ABTS/NBT). After comparing the different UV–vis absorbances of the PAA@MPDA NPs containing sample and control radical solution, the high radical scavenging abilities, and scavenging activity was calculated (Fig. 3a−c), and they displayed a dose-dependent manner (Fig. S4a−c). In contrast, the positive group exhibited significant signals of DPPH, •OH, and $\bullet O_2^-$ radicals, supporting the efficient redox medium activity of PAA@MPDA NPs. All the above-mentioned results established a good foundation for the antioxidant application of nanoparticles in organisms.

In addition, PAA@MPDA NPs can be used as an ideal drug carrier based on plentiful aromatic rings in PDA. To confirm the drug transport process in vivo after oral administration, the changes in the surface and morphology of the PAA@MPDA NPs in the simulated gastric and intestinal fluids were verified, respectively. As shown in Fig. 3d-**e**, the PAA@MPDA NPs were positively charged (1.2 ± 0.4) and the PAA was tightly wrapped on the surface of the MPDA NPs in the simulated gastric

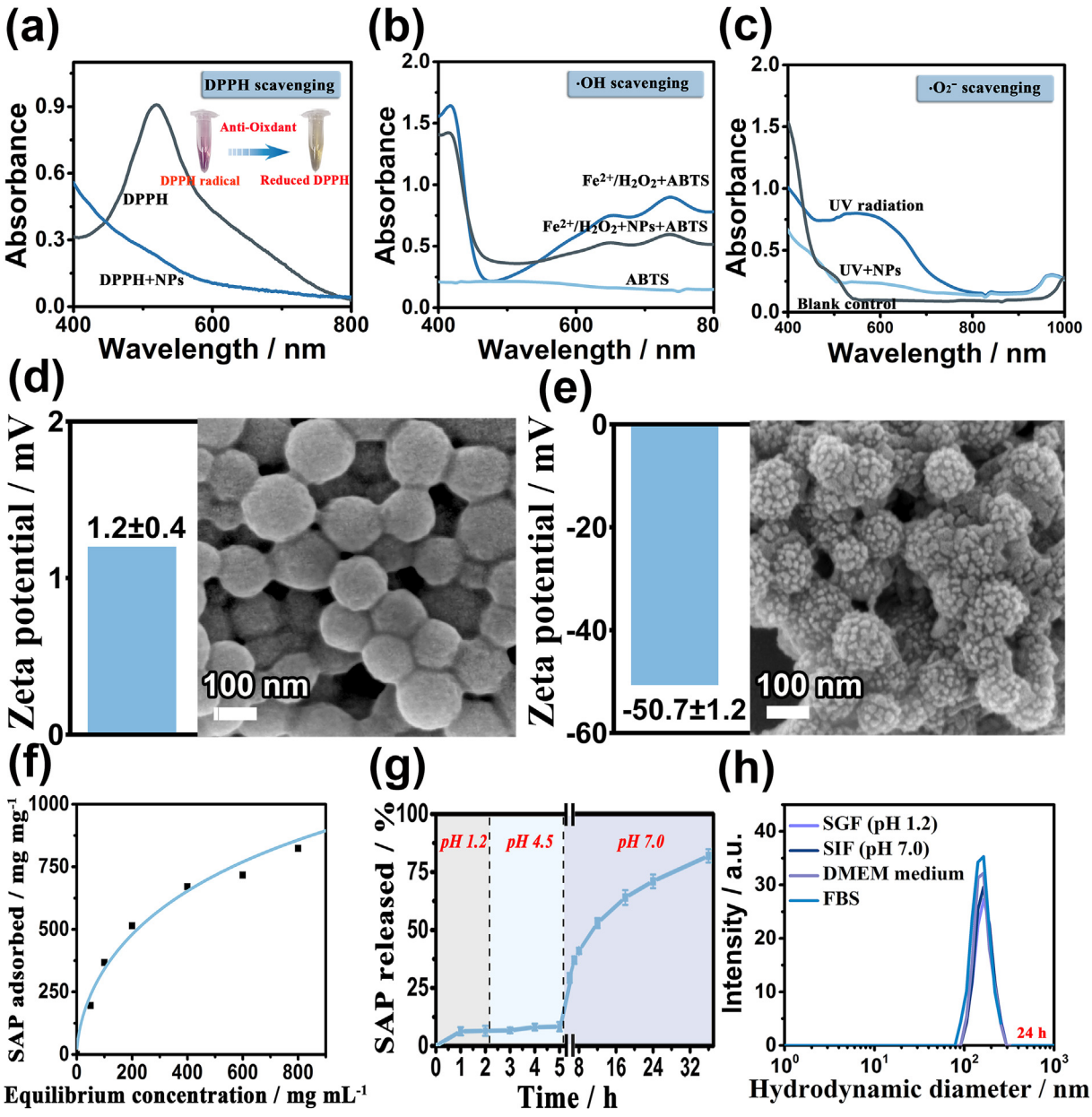

Fig. 3. ROS scavenging and pH-responsive drug release capacity of PAA@MPDA NPs. Radical scavenging of PAA@MPDA NPs toward (a) DPPH radicals, (b) •OH radicals and (c) $\bullet O_2^-$ radicals. Zeta potential data (left) and SEM images (right) of PAA@MPDA after 24 h incubation in (d) pH 1.2 and (e) pH 7.0 for 24 h, respectively. (f) Adsorption isotherm of SAP on PAA@MPDA, obtained by varying the initial SAP concentrations (0–2 mg mL^{-1}); (g) stimuli responsive SAP release from PAA@MPDA at different pH conditions: pH 1.2, pH 4.5, and pH 7.0. (h) Hydrodynamic diameter distributions of PAA@MPDA NPs in SGF (pH 1.2), SIF (pH 7.0), DMEM medium and FBS for 24 h.

fluid (SGF, pH 1.2), while PAA@MPDA NPs were negatively charged (-50.7 ± 1.2) and the pore structure extends leaks out in the simulated intestinal fluid (SIF, pH 7.0). This structural change could prevent the drug from being degraded or released prematurely during transport. Then, an anti-inflammatory drug (sulfasalazine, SAP) as a model drug to investigate the drug loading capacity of PAA@MPDA NPs under alkaline conditions (Fig. 3f). The PAA@MPDA NPs loaded with large amounts of SAP (928 μg mg^{-1}) to form a composite nanomedicine (PAA@MPDA-SAP NPs) due to the π-π stacking and hydrophobic interactions between the abundant aromatic rings in the PDA and SAP. Subsequently, the drug release behavior of PAA@MPDA-SAP NPs was simulated at different pH conditions in vitro (Fig. 3g). The SAP was released in the medium at pH 1.2 and 4.5 (<17%). Once the pH value was increased to 7.0, the SAP was rapidly released and the release amount reached ~82% after 36 h. This behavior could be explained by the carboxylic function groups of the PAA polymer starting to be de-protonated at these pH values (pKa≈5) [44]. When the pH < pKa, PAA chains would be neutral and would tend to shrink and exhibit a relatively hydrophobic behavior, while when the pH > pKa, the chains would begin to dissolve and swell. Therefore, the PAA shell can effectively prevent the early release of SAP in the stomach, and PAA@MPDA NPs can be used as an ideal drug carrier for oral delivery of anti-inflammatory drugs.

Furthermore, we conducted a stability study for PAA@MPDA NPs. It is showed that the particle sizes of the PAA@MPDA NPs were relatively stable during incubation in SGF, SIF, DMEM medium, and 10% FBS for 24 h (Figs. 3h) and 48 h (Fig. S5) at 37 °C, respectively. Overall, the above results demonstrate that the PAA@MPDA NPs exhibited good biological stability, efficient drug loading capacity, and good ROS scavenging ability, possessing a potential for being the formulation for synergistic treatment of IBD.

3.3. Cellular uptake and relief of inflammation by PAA@MPDA-SAP NPs in a Co-culture cell model

The anti-inflammatory effects due to PAA@MPDA-SAP NPs were evaluated at the cellular level. First, the internalization of PAA@MPDA NPs with RAW264.7 was investigated by Bio-TEM. As shown in Fig. 4a and b, after incubation with PAA@MPDA NPs, some vesicles were present in the cytoplasm, and many NPs could be found in these vesicles, indicating that the hybrid nanoparticles could be phagocytized by the RAW264.7 through endocytosis. Then, the uptake pathways of PAA@MPDA NPs were explored by ways of confocal laser scanning microscopy and flow cytometry (Fig. S6). The results indicate that PAA@MPDA NPs readily enter and accumulate in cells in high quantities using the same two endocytic pathways: mostly by macropinocytosis and partially by clathrin-mediated endocytosis. Furthermore, the biocompatibility of the PAA@MPDA NPs on RAW264.7 and Caco-2 cells and SAP/PAA@MPDA-SAP NPs on Caco-2 cells with different concentrations for 24 h was determined by the CCK-8 assay. As shown in Fig. S7a, PAA@MPDA NPs (0−200 μg mL^{-1}) did not exhibit cytotoxicity after incubation for 24 h, indicating the high biocompatibility of the nanocarrier system and the PAA@MPDA-SAP NPs could reduce the toxicity caused by SAP (Fig. S7b).

Subsequently, the Caco-2 and RAW 264.7 cells co-culture model was established to evaluate the anti-inflammation effects of PAA@MPDA-SAP NPs. As shown in Fig. 4c, a cellular inflammation model was established by treating RAW 264.7 cells with LPS (100 ng mL^{-1}) for 12 h (Fig. S8), and the Caco-2 cells were co-cultured PAA@MPDA-SAP NPs to investigate the properties of the nanocarrier system with respect to both scavenging of ROS and the anti-inflammatory effects. After stimulation, the expression of inflammatory factors in RAW 264.7 cells changed significantly (Fig. S9), and the expression level of ROS in Caco-2 cells was monitored by confocal microscopy (CLSM). As depicted in Fig. 4d, An ROS-sensitive fluorescent probe (DCFH-DA) was applied to detect ROS expression levels. After LPS treatment, Caco-2 cells in co-culture cell model showed an obvious green fluorescence signal, and the green fluorescence signals were significantly weakened after co-incubation of PAA@MPDA-SAP NPs due to the synergy between PAA@MPDA NPs and SAP. This finding was also observed for quantitative flow cytometry analysis (Fig. 4e and Fig. S10). It is shown that the nanocarrier system plays a synergistic role through the scavenging effect of ROS and the release of anti-inflammatory drugs.

To further investigate the anti-inflammatory effect of the NPs system, both proinflammatory (IL-1β, IL-6, TNF-α) and anti-inflammatory cytokines (IL-10) were measured in Caco-2 by qPCR and ELISA assay. The PAA@MPDA-SAP NPs exhibited a better anti-inflammatory effect than direct administration of SAP and PAA@MPDA ($p < 0.0001$) (Fig. 4g–j and Fig. S11). When inflammatory cytokines are out of balance, the integrity of the intestinal epithelial cell monolayers will be damaged. To determine the preventive effects of NPs on the integrity of colonic epithelial cells, we investigated the intestinal epithelial barrier of Caco-2 cells by the transepithelial electrical resistance (TEER). As shown in Fig. 4f, LPS stimulation for 12 h led to a 2.15-fold decrease of the TEER in the Caco-2 cells as compared with the control group. However, the PAA@MPDA-SAP NPs almost perfectly redeemed the LPS-induced TEER decline. These results suggest that the NP system exerted a good effect on scavenging ROS and inhibiting inflammatory cytokines.

3.4. PAA@MPDA-SAP NPs alleviates DSS-induced colitis

Oral nanomedicine must overcome the degradation of gastric acid and digestive enzymes in order to reach the colon to exert their therapeutic effect [45]. Therefore, to observe the efficacy of PAA@MPDA-SAP NPs in vivo, we established DSS-induced mouse colitis model. As shown in Fig. 5a, mice were given 2.5% DSS in drinking water for 7 consecutive days and with drinking water being freely available for two days to induce colitis. In the early stage of colitis, mice were administered orally SAP, PAA@MPDA NPs, and PAA@MPDA-SAP NPs (10 mg kg^{-1}) on predetermined days, respectively. First, the nanocarrier was modified with IR780 iodide to investigate the distribution of PAA@MPDA NPs in vivo after oral administration. The IVIS imaging results revealed that considerable accumulation of the PAA@MPDA-IR780 NPs in the colonic tissue after oral administration to colitis mice (Fig. 5b). Based on the high amounts of positively charged proteins in the inflamed colon, the negatively charged PAA@MPDA NPs could be enriched efficiently at the region with colonic inflammation via electrostatic interactions. The IVIS imaging also demonstrated the transit of PAA@MPDA-IR780 NPs in the colon (Fig. S12). The results showed that, with the prolongation of the transit time, the PAA@MPDA-IR780 NPs were effectively enriched in the colon within 8 h but then there was a gradual downward shift after 12 h.

Moreover, the therapeutic efficacy was evaluated with respect to body weights, disease activity indexes (DAIs), colon lengths, rectal areas, and mini-endoscopic and histological observation of colon [46]. As shown in Fig. 5c, the body weight of the DSS-induced colitis mice decreased by about 38% throughout disease progression. However, the body weight of the PAA@MPDA-SAP NPs-treated group had just decreased by 12%. Correspondingly, PAA@MPDA-SAP NPs-treated mice showed a longer colon length and a lower DAI compared to the DSS-treated group (Fig. 5d, **S13, and S14**). As displayed in Fig. 5e, the results of rectal area observation showed that there was obvious congestion, redness, and swelling around the anus in the DSS-treated mice. Meanwhile, multiple ulcers of intestinal mucosa were observed in the DSS-induced mice via mini-endoscopic imaging, which has been considered one of the typical symptoms of UC. However, these symptoms both were alleviated after PAA@MPDA-SAP NPs treatment. Additionally, the H&E-stained colon tissues showed that there were obvious pathological ruptures and inflammatory infiltration in DSS group. The treatment of SAP and PAA@MPDA NPs separately both reduced inflammatory infiltrations. However, the effect of PAA@MPDA-SAP NPs treatment showed that the inflammatory infiltration was almost reduced to close to the healthy group. These results suggest that PAA@MPDA-SAP NPs can effectively alleviate the symptoms of colitis by highly enriching and releasing the NPs system at the site of colonic inflammation.

3.5. PAA@MPDA-SAP NPs against DSS-induced colitis through inhibiting inflammatory factors, scavenging ROS, and maintaining intestinal barrier

To further understand the mechanism of PAA@MPDA-SAP NPs in the treatment of IBD, the key elements which affected the occurrence of enteritis were examined. First, inflammatory factors in colon tissue were detected by qPCR and ELISA assay. The treatment of SAP and PAA@MPDA NPs both decreased the expression of proinflammatory factors (IL-1β, IL-6, and TNF-α), and the PAA@MPDA-SAP NPs-treated group showed the lowest expression of them among all the treatment groups (Fig. 6a–c and Fig. S15 a-c). Moreover, the expression of anti-inflammatory factor (IL-10) showed an opposite varying trend (Fig. 6d and Figure S15 d). Next, we investigated the antioxidant effects. With the treatment of PAA@MPDA-SAP NPs, the ROS was almost eliminated in the healthy control group (Fig. 6e). Anti-oxidase SOD and myeloperoxidase (MPO) were also detected in the colon tissue after various treatments. It is shown that PAA@MPDA-SAP NPs-treated group resulted in an increase in the SOD content and a decrease in the MPO content (Fig. S16). Given that, under inflammatory conditions, the nanomedicines were first enriched in the damaged intestinal epithelial tissue through the e-EPR effect. Therefore, we further extracted mouse colonic epithelial cells and again detected the expression of inflammatory factors. The results showed the same changes in inflammatory cytokines in colonic epithelial cells as in colon tissue (Fig. S17).

It is well known that the tight junction proteins (TJs) composed of transmembrane barrier (e.g., ZO-1, Occludin, and Claudin-1) play an important role in the pathogenesis of IBD. The destruction of the TJs is one of the most prominent features and will lead to cascade inflammation in the development of IBD [47,48]. Therefore, we investigated the

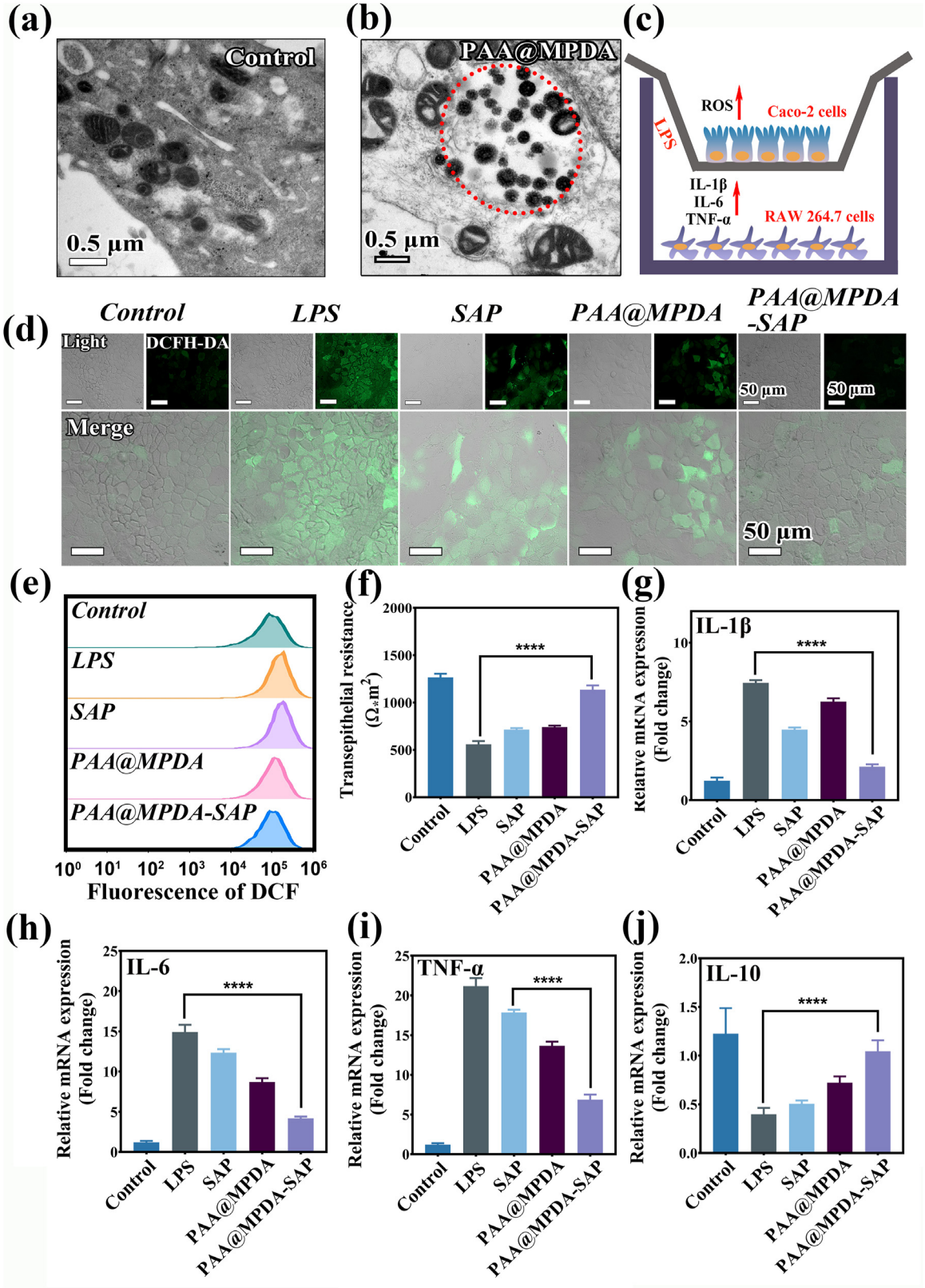

Fig. 4. Evaluation of ROS-scavenging and anti-inflammation ability in co-culture system. TEM of (a) RAW264.7 and (b) co-incubated with PAA@MPDA NPs for 24 h. (c) Experimental design of the LPS-induced inflammation model. (d) CLSM images of Caco-2 cells after treatment with LPS (100 ng mL^{-1}) and other treatments. Scale bar: 50 μm. (e) Flow cytometry for levels of intracellular after various treatments. (f)TEER measurements for Caco-2 cells on filters during various treatments. One representative experiment is shown with mean ± SD for six wells. The relative expression levels of (g) IL-1β, (h) IL-6, (i) TNF-α and (j)IL-10 in LPS-induced co-incubation after the indicated treatments. Data are presented as mean ± SD (n = 6). (****$p < 0.0001$).

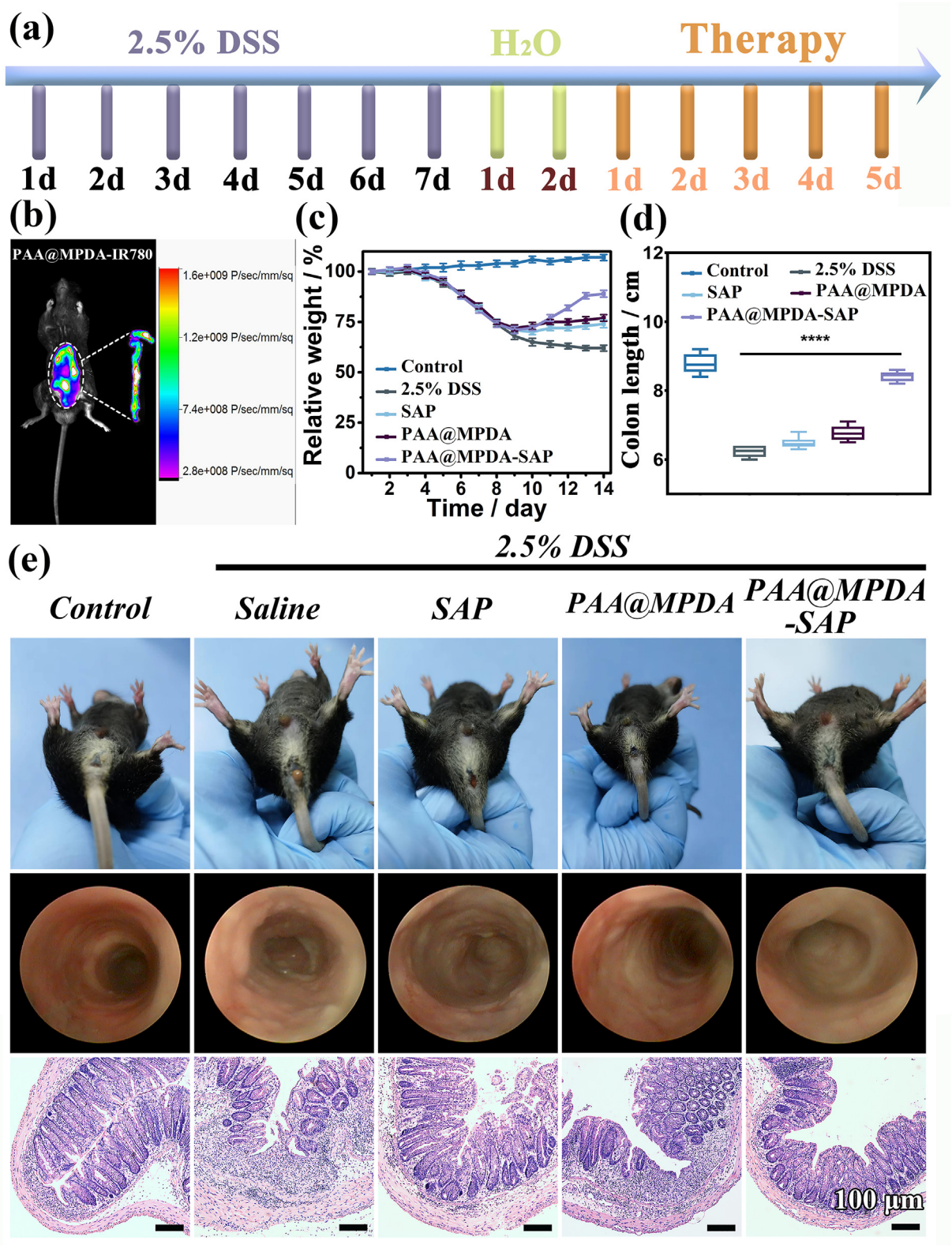

Fig. 5. In vivo therapeutic efficiency of PAA@MPDA-SAP NPs. (a) Experimental design of the DSS-induced mouse model. (b) IVIS imaging of mouse with DSS-induced colitis after treatments of PAA@MPDA-IR780 NPs. (c) Variations of body weight over time. (d) Colon length of mice from various groups. (e) Representative photographs of rectal areas of a healthy mouse, mini-endoscopic images and H&E-stained colonic pathological sections of colons from different mouse groups. Scale bars: 100 μm. Error bars represent means ± SD (n = 8) (****$p < 0.0001$).

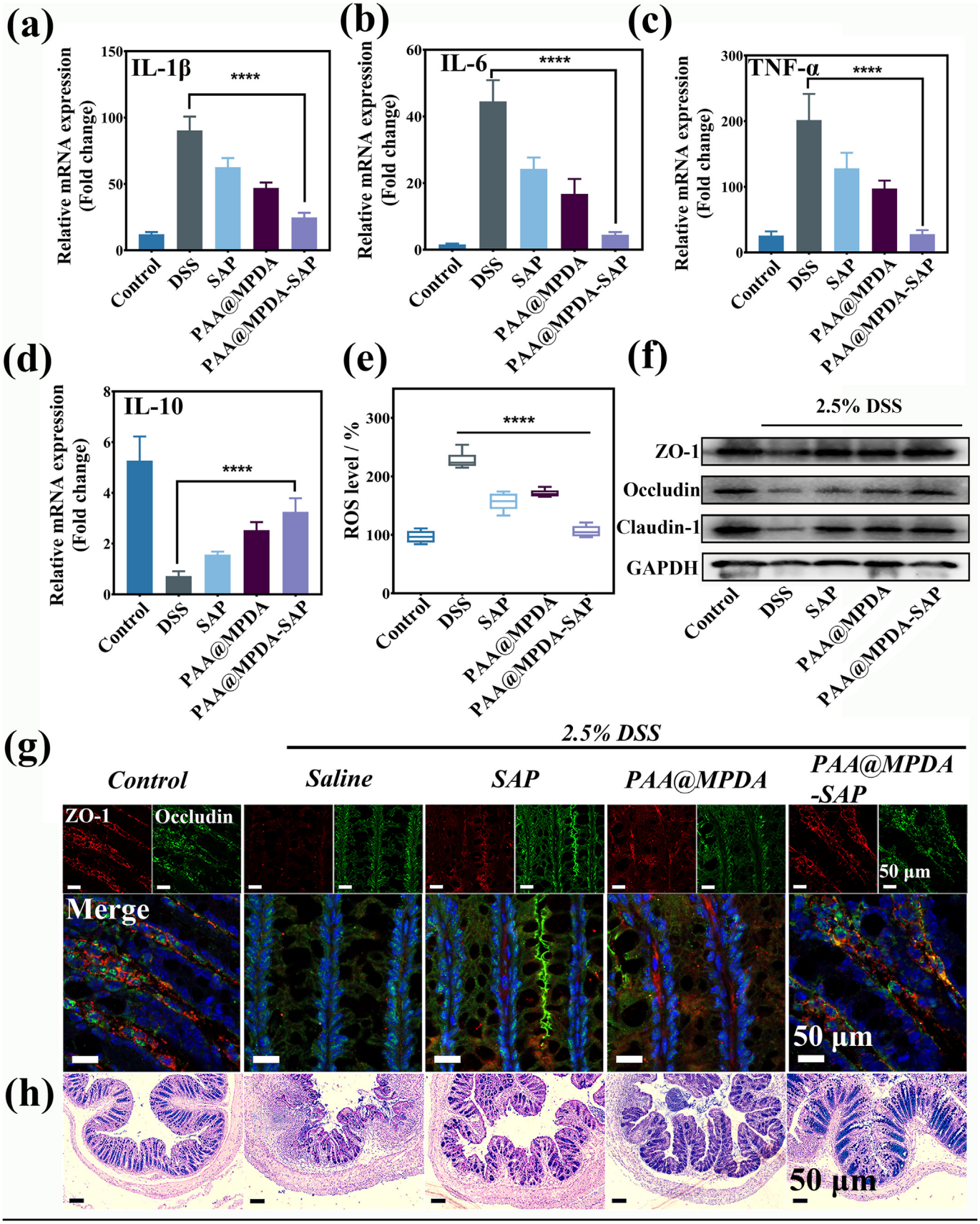

Fig. 6. In vivo retardation effect of PAA@MPDA-SAP NPs. Relative expression levels of (a) IL-1β, (b) IL-6, (c) TNF-αand (d) IL-10 in DSS-induced colitis after indicated treatments. Error bars represent means ± SD (n = 8). (e) ROS level of homogenized colonic tissue. (f) Western blot analysis of TJ proteins expression in the colonic mucosa. (g) Immunofluorescent staining for the expression of ZO-1 and Occludin in colon tissue for various treatments. (h) AB-PAS staining of colon tissue for various treatments. Scale bar = 50 μm. (****$p < 0.0001$).

expression of TJs via western blot and immunofluorescence separately. As shown in Fig. 6f, the PAA@MPDA-SAP NPs-treated group observably inhibit the decrease in the TJs expression caused by the DSS. ZO-1 is a peripheral membrane protein, which interacts with Occludin to maintain TJs integrity. So, fluorescence staining was used to observe the integrity of ZO-1 and Occludin in colon tissues. The finding showed that ZO-1 and Occludin had the same results, and both recovered good integrity in the PAA@MPDA-SAP NPs-treated group compared to DSS-treated group (Fig. 6g).

In addition to TJs, the mucus layer is also part of an important protective barrier of colon, which is thinning or even fully destroyed in colitis tissues [48]. Mucus is secreted by goblet cells and includes neutral and acidic mucus, which prevents the direct physical contact of epitheliums from microbiota [48]. Alcian blue and periodic acid-Schiff (AB-PAS) staining was usually used to analyze the number of goblet cells and the depth of crypts, which reflected the mucus barrier. As displayed in Fig. 6h, there was a significantly strong mucous layer staining in the colon tissue of PAA@MPDA-SAP NPs-treated group compared with other treatment groups. These results suggest that the PAA@MPDA-SAP NPs can promote the restoration of enteritis mainly by inhibiting inflammatory factors, scavenging ROS, and maintaining intestinal barrier.

3.6. *In vivo biosafety assessment of PAA@MPDA NPs*

With reference to biological safety, it is necessary to study the potential toxicity of the as-prepared NPs toward normal tissue. As depicted in Fig. 7a, there was negligible inflammatory infiltration and cell damage bae on inspection of the H&E staining. Furthermore, the PAA@MPDA NPs treatment did not induce significant changes in the blood biochemical analysis data (Fig. 7b–f). The toxicity of PAA@MPDA NPs at a 10-fold higher dose (10 mg kg^{-1}) than that used in the above therapeutic experiments (1 mg kg^{-1}) was investigated. As shown in Fig. 7g, there were no significant changes in levels of aspartate aminotransferase (AST) and alanine aminotransferase (ALT) among all the groups. These results suggest that the PAA@MPDA NPs had a good biosafety profile and were able to relieve intestinal inflammation in DSS-induced colitis without adverse effects.

3.7. *PAA@MPDA-SAP NPs cytotoxicity and efficacy in human colon organoids*

The PAA@MPDA-SAP NPs treatment inhibited inflammation and maintained intestinal barrier in intestinal epithelial cells under in vitro conditions and animal models. However, growing evidence has shown that not only do traditional two-dimensional (2D) cell cultures fail to recapitulate cell-cell interactions due to species differences, but also animal models fail to fully reflect human physiological processes [49]. Human induced pluripotent stem cells (hiPSCs)-derived intestinal organoids, which more accurately mimic realistic gut architectures, preserve the physiological characteristics of the digestive system, and are a powerful tool for validating drugs and in vivo data [49]. Therefore, we planned to examine the efficacy of PAA@MPDA-SAP NPs on human colon organoid model. First, the organoids were obtained from human colon tissue cultured in vitro (Fig. S18). Next, the toxicity of PAA@MPDA-SAP NPs was tested via the CellTiter-Glo assay system in normal human colon organoids. It was shown that the PAA@MPDA NPs

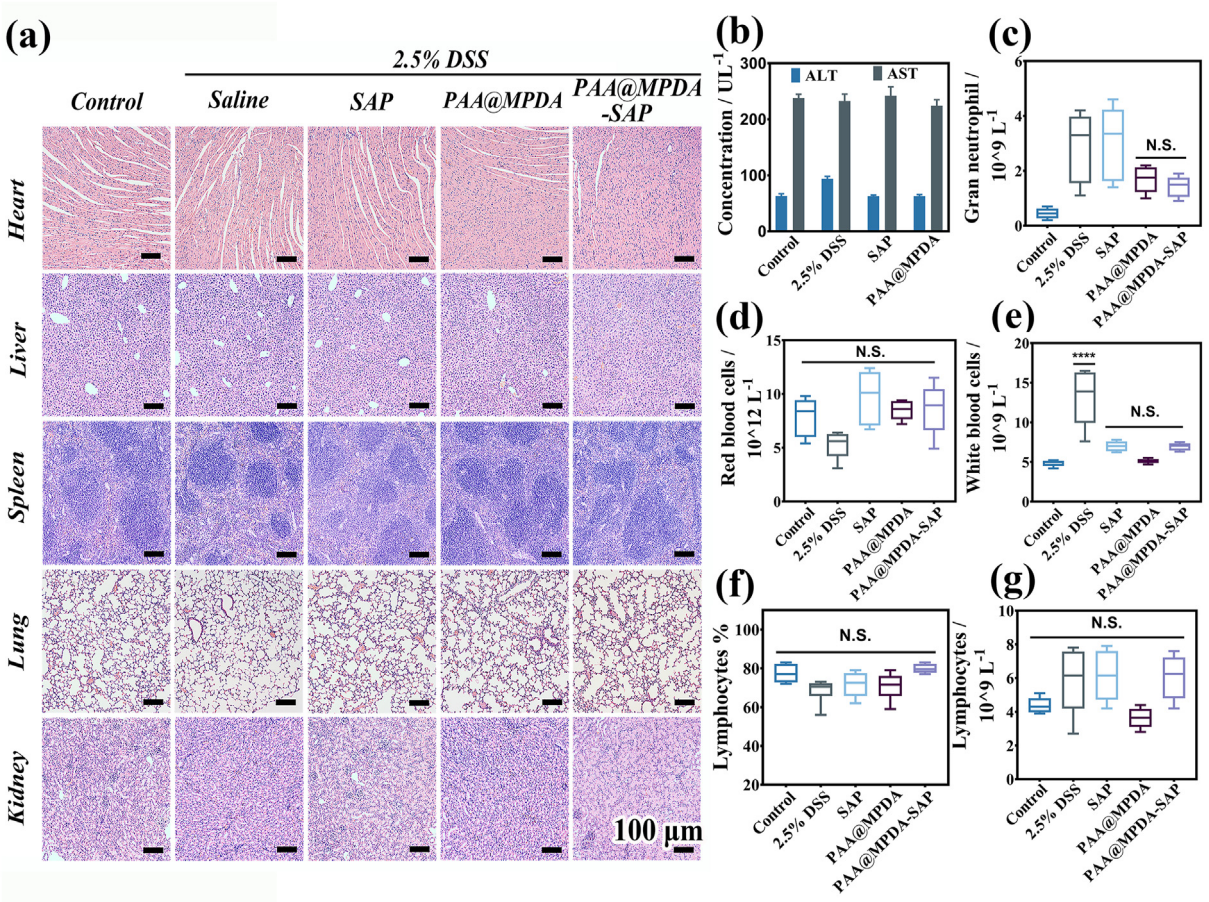

Fig. 7. Biocompatibility testing of PAA@MPDA NPs. (a) H&E-stained major organ slices harvested from various mouse groups. Scale bar = 100 μm. (b) AST and ALT levels in the serum of mice after intrarectal administration of 2.5% DSS, 100 μL of saline, SAP and PAA@MPDA NPs (dose 10 mg kg^{-1} mice), respectively. (c–g) Blood parameters from various mouse groups. Data are presented as the mean ± SD (n = 8) (****$p < 0.0001$; NS not significant).

and MPDA NPs caused negligible cytotoxicity after co-incubation with organoids for 24 and 48 h (Fig. S19). Efficient uptake of the nanomedicine is the first step towards treatment of inflammation, so Bio-TEM was performed to investigate the internalization of PAA@MPDA NPs in human colon organoids. As shown in Fig. 8a and b, a substantial quantity of the PAA@MPDA NPs was taken up by the organoids after co-incubation for 24 h. To correlate our animal experimental data related to the efficacy of PAA@MPDA-SAP NPs, the anti-inflammatory and intestinal barrier protective effects were examined in colon organoids. Consistent with our in vitro and mouse results, the PAA@MPDA-SAP NPs

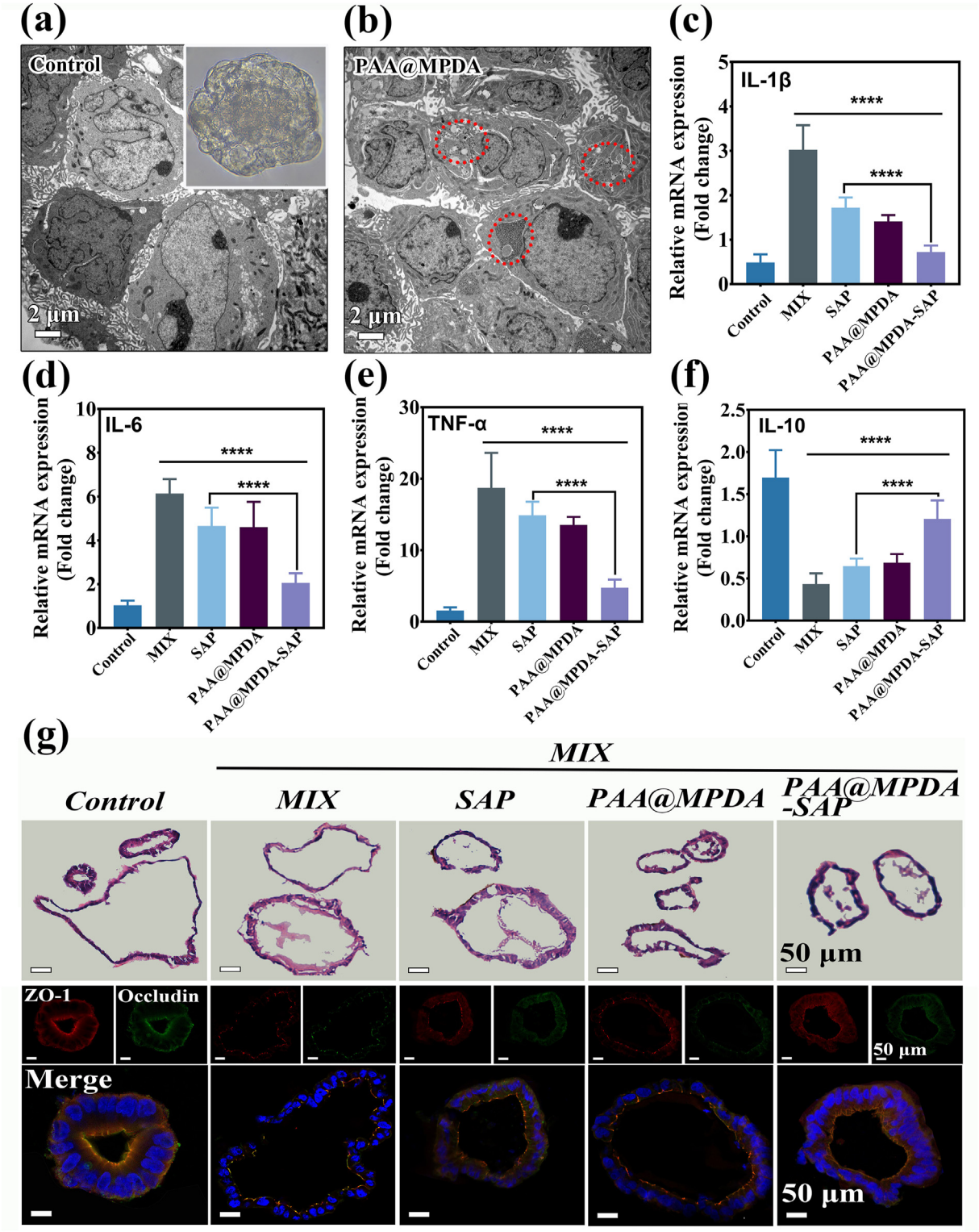

Fig. 8. Therapeutic efficiency of PAA@MPDA-SAP NPs in human colon organoids. TEM image of (a) colon organoids and (b) colon organoids co-incubated with PAA@MPDA NPs for 24 h, respectively. Inset: the close-up inverted microscope image for the growth of the colon organoid for 7 days. Relative expression levels of (c) IL-1β, (d) IL-6, (e) TNF-α and (f) IL-10 in MIX-induced colon organoids after indicated treatments. Data are presented as mean ± SD (n = 6). (g) H&E, TJs proteins (ZO-1 and Occludin)-stained human colon organoids from different groups. Scale bar = 50 μm. (****$p < 0.0001$).

treatment inhibited significantly the levels of pro-inflammatory cytokines under a strong cocktail of inflammatory mediators (Mix) stimulation (Fig. 8c–f). Similarly, H&E-stained organoid structure and fluorescence-stained TJs both indicated that PAA@MPDA-SAP NPs had a good effect on intestinal barrier repair compared control group (Fig. 8g). These results suggest that PAA@MPDA-SAP NPs could attenuate enteritis in a preclinical model.

4. Conclusions

In summary, a novel nanomedicine of PAA@MPDA-SAP NPs that is effective in treatment of IBD has been developed by synergistic effect of anti-inflammation and anti-oxidation. The PAA@MPDA NPs displayed efficient SAP loading and ROS scavenging capacity. After oral administration, the negatively charged PAA@MPDA-SAP NPs adhered preferentially to inflamed intestines in both colitis induced mice or organoid specimens of human colon and released SAP at the inflammatory site of colon. The PAA@MPDA-SAP NPs exhibited superior therapeutic effects than free SAP and PAA@MPDA NPs by synergy reducing the inflammatory cytokines and the expression of ROS. Moreover, the PAA@MPDA NPs had a greatly reduced systemic exposure, a good safety profile and served as a functional and effective synergistic therapy for treatment of IBD.

Credit author statement

Haidi Guan: Experimental operation, Data curation, Writing – original draft, Conceptualization. Zhongwei Xu: Experimental operation, Data curation, Formal analysis. Guangsheng Du: Specimen collection. Qinghua Liu: Experimental operation. Qianshan Tan: Experimental operation. Yihui Chen: Methodology. Shuaishuai Chen: Project administration. Jingfeng Wu: Methodology, Instrument provision. Fengchao Wang: Instrument provision. Jixi Zhang: Writing – review. Lihua Sun: Writing – review & editing, Funding acquisition, Project administration. Weidong Xiao: Funding acquisition, Conceptualization, Supervision.

Declaration of competing interest

The authors declare that they have no known competing financial interests or personal relationships that could have appeared to influence the work reported in this paper.

Data availability

Data will be made available on request.

Acknowledgments

This work was supported by grants from the National Natural Science Foundation of China (NSFC 81873933 to L.H.S, NSFC 82270585 to W.D.X) and Army Medical University project (CX2019JS212 to W.D.X/2021XJS25 to W.D.X).

Appendix A. Supplementary data

Supplementary data to this article can be found online at https://doi.org/10.1016/j.mtbio.2023.100610.

References

[1] A.R. Bourgonje, T. Vogl, E. Segal, R.K. Weersma, Antibody signatures in inflammatory bowel disease: current developments and future applications, Trends Mol. Med. 28 (2022) 693–705. https://www.sciencedirect.com/science/article/pii/S1471491422001125.

[2] H. Luo, G. Cao, C. Luo, D. Tan, C.T. Vong, Y. Xu, S. Wang, H. Lu, Y. Wang, W. Jing, Emerging pharmacotherapy for inflammatory bowel diseases, Pharmacol. Res. 178 (2022), 106146. https://www.sciencedirect.com/science/article/pii/S1043661822000913.

[3] A. Sinha, Y. Li, M.K. Mirzaei, M. Shamash, R. Samadfam, I.L. King, C.F. Maurice, Transplantation of bacteriophages from ulcerative colitis patients shifts the gut bacteriome and exacerbates the severity of dss colitis, Microbiome 10 (2022) 105, https://doi.org/10.1186/s40168-022-01275-2.

[4] M.E. Kuenzig, S.G. Fung, L. Marderfeld, J.W.Y. Mak, G.G. Kaplan, S.C. Ng, D.C. Wilson, F. Cameron, P. Henderson, P.G. Kotze, J. Bhatti, V. Fang, S. Gerber, E. Guay, S. Kotteduwa Jayawarden, L. Kadota, F. Maldonado D, J.A. Osei, R. Sandarage, A. Stanton, M. Wan, J. Bhatti, S. Gerber, E. Guay, S.K. Jayawarden, L. Kadota, F. Maldonado, E. Maltus, S. Bhattacharya, J. Osei, R. Sandarage, A. Stanton, M. Wan, E.I. Benchimol, Twenty-first century trends in the global epidemiology of pediatric-onset inflammatory bowel disease: systematic review, Gastroenterology 162 (2022) 1147–1159.e4. https://www.sciencedirect.com/science/article/pii/S0016508522000026.

[5] J.N. Peña-Sánchez, J.A. Osei, J.D. Marques Santos, D. Jennings, M. Andkhoie, C. Brass, G. Bukassa-Kazadi, X. Lu, M. Johnson-Jennings, L. Porter, R. Porter, C.-L. Quintin, R. Sanderson, U. Teucher, S. Fowler, Increasing prevalence and stable incidence rates of inflammatory bowel disease among first nations: population-based evidence from a western canadian province, Inflamm. Bowel Dis. 28 (2021) 514–522, https://doi.org/10.1093/ibd/izab096.

[6] R. Deshmukh, R.K. Harwansh, S.D. Paul, R. Shukla, Controlled release of sulfasalazine loaded amidated pectin microparticles through eudragit s 100 coated capsule for management of inflammatory bowel disease, J. Drug Deliv. Sci. Technol. 55 (2020), 101495. https://www.sciencedirect.com/science/article/pii/S1773224719315576.

[7] A. Yousefi-Ahmadipour,S. Ebrahimi-Barough, S. Niknia, A. Allahverdi, A. Mirzahosseini-pourranjbar, M. Tashakori, S. Khajouee Ravari, F. Asadi, R. Heidari Barchi Nezhad, N. Lotfibakhshaiesh, M.R. Mirzaei, Therapeutic effects of combination of platelet lysate and sulfasalazine administration in tnbs-induced colitis in rat, Biomed. Pharmacother. 125 (2020), 109949. https://www.sciencedirect.com/science/article/pii/S0753332220301396.

[8] O.H. Nielsen, L.K. Munck, Drug insight: aminosalicylates for the treatment of ibd, Nat. Clin. Pract. Gastroenterol. Hepatol. 4 (2007) 160–170, https://doi.org/10.1038/ncpgasthep0696.

[9] C. Li, Y. Zhao, J. Cheng, J. Guo, Q. Zhang, X. Zhang, J. Ren, F. Wang, J. Huang, H. Hu, R. Wang, J. Zhang, A proresolving peptide nanotherapy for site-specific treatment of inflammatory bowel disease by regulating proinflammatory microenvironment and gut microbiota, Adv. Sci. 6 (2019), 1900610. https://onlinelibrary.wiley.com/doi/abs/10.1002/advs.201900610.

[10] S. Liu, Y. Cao, L. Ma, J. Sun, L. Ramos-Mucci, Y. Ma, X. Yang, Z. Zhu, J. Zhang, B. Xiao, Oral antimicrobial peptide-egcg nanomedicines for synergistic treatment of ulcerative colitis, J. Contr. Release 347 (2022) 544–560. https://www.sciencedirect.com/science/article/pii/S0168365922002887.

[11] N. Kulkarni, P. Jain, A. Shindikar, P. Suryawanshi, N. Thorat, Advances in the colon-targeted chitosan based multiunit drug delivery systems for the treatment of inflammatory bowel disease, Carbohydr. Polym. 288 (2022), 119351. https://www.sciencedirect.com/science/article/pii/S0144861722002557.

[12] D.-f. Li, M.-f. Yang, H.-m. Xu, M.-z. Zhu, Y. Zhang, C.-m. Tian, Y.-q. Nie, J.-y. Wang, Y.-j. Liang, J. Yao, L.-s. Wang, Nanoparticles for oral delivery: targeted therapy for inflammatory bowel disease, J. Mater. Chem. B 10 (2022) 5853–5872, https://doi.org/10.1039/D2TB01190E.

[13] G. Fang, B. Tang, Current advances in the nano-delivery of celastrol for treating inflammation-associated diseases, J. Mater. Chem. B 8 (2020) 10954–10965, https://doi.org/10.1039/D0TB01939A.

[14] C. Xu, S. Chen, C. Chen, Y. Ming, J. Du, J. Mu, F. Luo, D. Huang, N. Wang, Z. Lin, Z. Weng, Colon-targeted oral nanoparticles based on ros-scavenging hydroxyethyl starch-curcumin conjugates for efficient inflammatory bowel disease therapy, Int. J. Pharm. 623 (2022), 121884. https://www.sciencedirect.com/science/article/pii/S0378517322004392.

[15] H. Hadji, K. Bouchemal, Advances in the treatment of inflammatory bowel disease: focus on polysaccharide nanoparticulate drug delivery systems, Adv. Drug Deliv. Rev. 181 (2022), 114101. https://www.sciencedirect.com/science/article/pii/S0169409X21004944.

[16] T. Sun, C.H.T. Kwong, C. Gao, J. Wei, L. Yue, J. Zhang, R.D. Ye, R. Wang, Amelioration of ulcerative colitis via inflammatory regulation by macrophage-biomimetic nanomedicine, Theranostics 10 (2020) 10106–10119. https://www.thno.org/v10p10106.htm.

[17] C. Gao, Q. Huang, C. Liu, C.H.T. Kwong, L. Yue, J.-B. Wan, S.M.Y. Lee, R. Wang, Treatment of atherosclerosis by macrophage-biomimetic nanoparticles via targeted pharmacotherapy and sequestration of proinflammatory cytokines, Nat. Commun. 11 (2020) 2622, https://doi.org/10.1038/s41467-020-16439-7.

[18] S. Zhao, Y. Li, Q. Liu, S. Li, Y. Cheng, C. Cheng, Z. Sun, Y. Du, C.J. Butch, H. Wei, An orally administered ceo2@montmorillonite nanozyme targets inflammation for inflammatory bowel disease therapy, Adv. Funct. Mater. 30 (2020), 2004692. https://onlinelibrary.wiley.com/doi/abs/10.1002/adfm.202004692.

[19] J. Wang, Z. Tao, T. Tian, J. Qiu, H. Qian, Z. Zha, Z. Miao, Y. Ma, H. Wang, Polyoxometalate nanoclusters: a potential preventative and therapeutic drug for inflammatory bowel disease, Chem. Eng. J. 416 (2021), 129137. https://www.sciencedirect.com/science/article/pii/S1385894721007282.

[20] Y. Liu, Y. Cheng, H. Zhang, M. Zhou, Y. Yu, S. Lin, B. Jiang, X. Zhao, L. Miao, C.-W. Wei, Q. Liu, Y.-W. Lin, Y. Du, C.J. Butch, H. Wei, Integrated cascade nanozyme catalyzes in vivo ros scavenging for anti-inflammatory therapy, Sci. Adv. 6 (2020) eabb2695, https://www.science.org/doi/abs/10.1126/sciadv.abb2695.

[21] D.K.W. Ocansey, B. Pei, X. Xu, L. Zhang, C.V. Olovo, F. Mao, Cellular and molecular mediators of lymphangiogenesis in inflammatory bowel disease, J. Transl. Med. 19 (2021) 254, https://doi.org/10.1186/s12967-021-02922-2.
[22] H. Qiu, H. Gong, Y. Bao, H. Jiang, W. Tong, Reactive oxygen species-scavenging hollow mno2 nanozymes as carriers to deliver budesonide for synergistic inflammatory bowel disease therapy, Biomater. Sci. 10 (2022) 457–466, https://doi.org/10.1039/D1BM01525G.
[23] S. Lin, H. Zhao, C. Xu, P. Zhang, X. Mei, D. Jiang, Sulfasalazine-loaded nanoparticles for efficient inflammatory bowel disease therapy via ros-scavenging strategy, Mater. Des. 225 (2023), 111465. https://www.sciencedirect.com/science/article/pii/S0264127522010887.
[24] W. Wang, J. Zheng, H. Zhou, Q. Liu, L. Jia, X. Zhang, D. Ge, W. Shi, Y. Sun, Polydopamine-based nanocomposite as a biomimetic antioxidant with a variety of enzymatic activities for Parkinson's disease, ACS Appl. Mater. Interfaces 14 (2022) 32901–32913, https://doi.org/10.1021/acsami.2c06981.
[25] Z. Tang, Y. Miao, J. Zhao, H. Xiao, M. Zhang, K. Liu, X. Zhang, L. Huang, L. Chen, H. Wu, Mussel-inspired biocompatible polydopamine/carboxymethyl cellulose/polyacrylic acid adhesive hydrogels with uv-shielding capacity, Cellulose 28 (2021) 1527–1540, https://doi.org/10.1007/s10570-020-03596-7.
[26] H. Liu, X. Qu, H. Tan, J. Song, M. Lei, E. Kim, G.F. Payne, C. Liu, Role of polydopamine's redox-activity on its pro-oxidant, radical-scavenging, and antimicrobial activities, Acta Biomater. 88 (2019) 181–196. https://www.sciencedirect.com/science/article/pii/S174270611930145X.
[27] J. Hu, L. Yang, P. Yang, S. Jiang, X. Liu, Y. Li, Polydopamine free radical scavengers, Biomater. Sci. 8 (2020) 4940–4950, https://doi.org/10.1039/D0BM01070G.
[28] L. Wang, Z. Wang, Y. Pan, S. Chen, X. Fan, X. Li, G. Chen, Y. Ma, Y. Cai, J. Zhang, H. Yang, W. Xiao, M. Yu, Polycatechol-derived mesoporous polydopamine nanoparticles for combined ros scavenging and gene interference therapy in inflammatory bowel disease, ACS Appl. Mater. Interfaces 14 (2022) 19975–19987, https://doi.org/10.1021/acsami.1c25180.
[29] D. Wu, J. Zhou, X. Chen, Y. Chen, S. Hou, H. Qian, L. Zhang, G. Tang, Z. Chen, Y. Ping, W. Fang, H. Duan, Mesoporous polydopamine with built-in plasmonic core: traceable and nir triggered delivery of functional proteins, Biomaterials 238 (2020), 119847. https://www.sciencedirect.com/science/article/pii/S0142961220300934.
[30] Z. Han, M. Gao, Z. Wang, L. Peng, Y. Zhao, L. Sun, Ph/nir-responsive nanocarriers based on mesoporous polydopamine encapsulated gold nanorods for drug delivery and thermo-chemotherapy, J. Drug Deliv. Sci. Technol. 75 (2022), 103610. https://www.sciencedirect.com/science/article/pii/S1773224722005214.
[31] M. Gao, Z. Han, X. Zhang, X. Zou, L. Peng, Y. Zhao, L. Sun, Construction of double-shelled hollow ag2s@polydopamine nanocomposites for fluorescence-guided, dual stimuli-responsive drug delivery and photothermal therapy, Nanomaterials 12 (2022) 2068. https://www.mdpi.com/2079-4991/12/12/2068.
[32] Y. Xing, J. Zhang, F. Chen, J. Liu, K. Cai, Mesoporous polydopamine nanoparticles with co-delivery function for overcoming multidrug resistance via synergistic chemo-photothermal therapy, Nanoscale 9 (2017) 8781–8790, https://doi.org/10.1039/C7NR01857F.
[33] T. Ding, Z. Wang, D. Xia, J. Zhu, J. Huang, Y. Xing, S. Wang, Y. Chen, J. Zhang, K. Cai, Long-lasting reactive oxygen species generation by porous redox mediator-potentiated nanoreactor for effective tumor therapy, Adv. Funct. Mater. 31 (2021), 2008573. https://onlinelibrary.wiley.com/doi/abs/10.1002/adfm.202008573.
[34] Y. Orooji, S. Mortazavi-Derazkola, S.M. Ghoreishi, M. Amiri, M. Salavati-Niasari, Mesopourous fe_3o_4@sio_2-hydroxyapatite nanocomposite: green sonochemical synthesis using strawberry fruit extract as a capping agent, characterization and their application in sulfasalazine delivery and cytotoxicity, J. Hazard Mater. 400 (2020), 123140. https://www.sciencedirect.com/science/article/pii/S0304389420311298.
[35] H. Guan, L. Wang, J. Zhang, Y. Xing, K. Cai, Selective enrichment of polydopamine in mesoporous nanocarriers for nuclear-targeted drug delivery, Part. Part. Syst. Char. 35 (2018), 1800011. https://onlinelibrary.wiley.com/doi/abs/10.1002/ppsc.201800011.
[36] S. Rajasekar, D.S.Y. Lin, L. Abdul, A. Liu, A. Sotra, F. Zhang, B. Zhang, Iflowplate—a customized 384-well plate for the culture of perfusable vascularized colon organoids, Adv. Mater. 32 (2020), 2002974. https://onlinelibrary.wiley.com/doi/abs/10.1002/adma.202002974.
[37] M. He, Z. Qin, X. Liang, X. He, B. Zhu, Z. Lu, Q. Wei, L. Zheng, A ph-responsive mesoporous silica nanoparticles-based drug delivery system with controlled release of andrographolide for oa treatment, Regen Biomater 8 (2021), https://doi.org/10.1093/rb/rbab020.
[38] M. Martínez-Carmona, D. Lozano, M. Colilla, M. Vallet-Regí, Lectin-conjugated ph-responsive mesoporous silica nanoparticles for targeted bone cancer treatment, Acta Biomater. 65 (2018) 393–404. https://www.sciencedirect.com/science/article/pii/S174270611730692X.
[39] R.S. Patil, E. Sancaktar, Fabrication of ph-responsive polyimide polyacrylic acid smart gating membranes: ultrafast method using 248 nm krypton fluoride excimer laser, ACS Appl. Mater. Interfaces 13 (2021) 24431–24441, https://doi.org/10.1021/acsami.1c01265.
[40] D. Wu, Z.-Q. Zhu, H.-X. Tang, Z.-E. Shi, J. Kang, Q. Liu, J. Qi, Efficacy-shaping nanomedicine by loading calcium peroxide into tumor microenvironment-responsive nanoparticles for the antitumor therapy of prostate cancer, Theranostics 10 (2020) 9808–9829. https://www.thno.org/v10p9808.htm.
[41] Y. Zhang, X. Wang, L. Ma, R. Tang, X. Zheng, F. Zhao, G. Tang, Y. Wang, A. Pang, W. Li, L. Wei, Polydopamine blended with polyacrylic acid for silicon anode binder with high electrochemical performance, Powder Technol. 388 (2021) 393–400. https://www.sciencedirect.com/science/article/pii/S0032591021003910.
[42] Y. Zhao, P. Xue, G. Lin, M. Tong, J. Yang, Y. Zhang, K. Ran, D. Zhuge, Q. Yao, H. Xu, A kpv-binding double-network hydrogel restores gut mucosal barrier in an inflamed colon, Acta Biomater. 143 (2022) 233–252. https://www.sciencedirect.com/science/article/pii/S174270612200126X.
[43] M. Cui, M. Zhang, K. Liu, Colon-targeted drug delivery of polysaccharide-based nanocarriers for synergistic treatment of inflammatory bowel disease: a review, Carbohydr. Polym. 272 (2021), 118530. https://www.sciencedirect.com/science/article/pii/S0144861721009176.
[44] C. Pan, X. Liu, K. Gong, F. Mumtaz, Y. Wang, Dopamine assisted pmoxa/paa brushes for their switchable protein adsorption/desorption, J. Mater. Chem. B 6 (2018) 556–567, https://doi.org/10.1039/C7TB02209C.
[45] M. Plaza-Oliver, M.J. Santander-Ortega, M.V. Lozano, Current approaches in lipid-based nanocarriers for oral drug delivery, Drug Delivery Translat. Res. 11 (2021) 471–497, https://doi.org/10.1007/s13346-021-00908-7.
[46] H. Wang, X. Huang, S. Xia, C. Chen, X. Chen, Y. Zhang, M.A. Farag, J. Xiao, S. Nie, Celery soluble dietary fiber antagonizes flavonoids ameliorative effect on dextran-sodium-sulfate-induced colitis in mice, J. Adv. Res. (2023). https://www.sciencedirect.com/science/article/pii/S2090123223000267.
[47] K. Parikh, A. Antanaviciute, D. Fawkner-Corbett, M. Jagielowicz, A. Aulicino, C. Lagerholm, S. Davis, J. Kinchen, H.H. Chen, N.K. Alham, N. Ashley, E. Johnson, P. Hublitz, L. Bao, J. Lukomska, R.S. Andev, E. Björklund, B.M. Kessler, R. Fischer, R. Goldin, H. Koohy, A. Simmons, Colonic epithelial cell diversity in health and inflammatory bowel disease, Nature 567 (2019) 49–55, https://doi.org/10.1038/s41586-019-0992-y.
[48] L. Sun, T. Li, H. Tang, K. Yu, Y. Ma, M. Yu, Y. Qiu, P. Xu, W. Xiao, H. Yang, Intestinal epithelial cells-derived hypoxia-inducible factor-1α is essential for the homeostasis of intestinal intraepithelial lymphocytes, Front. Immunol. 10 (2019). https://www.frontiersin.org/articles/10.3389/fimmu.2019.00806.
[49] T. Molnár, B. Jójárt, T. Resál, K. Szántó, D. Kata, I. Földesi, T. Molnár, J. Maléth, K. Farkas, P046 disease modelling of inflammatory bowel disease by human colon organoids, J. Crohns Colitis 15 (2021), https://doi.org/10.1093/ecco-jcc/jjab076.175. S155-S155.